NMR Structure of a Viral Peptide Inserted in Artificial Membranes

Marie Galloux, Sonia Libersou, Isabel Alves, Rodrigue Marquant, Gilmar Salgado, Human Rezaei, Jean Lepault, Bernard Delmas, Serge Bouaziz, Nelly Morellet

THE JOURNAL OF BIOLOGICAL CHEMISTRY VOL. 285, NO. 25, pp. 19409–19421, June 18, 2010

NMR Structure of a Viral Peptide Inserted in Artificial Membranes

A VIEW ON THE EARLY STEPS OF THE BIRNAVIRUS ENTRY PROCESS[*] [S]

Received for publication, October 19, 2009, and in revised form, March 8, 2010 Published, JBC Papers in Press, April 12, 2010, DOI 10.1074/jbc.M109.076083

Marie Galloux[‡§], Sonia Libersou[¶], Isabel D. Alves[‖], Rodrigue Marquant[‡], Gilmar F. Salgado[‖], Human Rezaei[§], Jean Lepault[¶], Bernard Delmas[§], Serge Bouaziz[‡], and Nelly Morellet[‡1]

From the [‡]Unité de Pharmacologie Chimique et Génétique, CNRS, UMR 8151, Faculté des Sciences Pharmaceutiques et Biologiques, Université Paris Descartes, 4 Avenue de l'Observatoire, Paris, F-75270 Cedex 06, the [§]Unité de Virologie et Immunologie Moléculaires, UR892, Bâtiment de Biotechnologies, INRA, Domaine de Vilvert, F-78350 Jouy-en-Josas, the [‖]UPMC Paris 06, CNRS, UMR 7203, Laboratoire des BioMolécules, FR 2769, Case Courier 182, 4 Place Jussieu, 75252 Paris Cedex 05, and the [¶]CNRS UMR 2472, INRA 1157, Virologie Moléculaire et Structurale, 1 Avenue de la Terrasse, F-91198 Gif-sur-Yvette, France

Nonenveloped virus must penetrate the cellular membrane to access the cytoplasm without the benefit of membrane fusion. For birnavirus, one of the peptides present in the virus capsid, pep46 for infectious bursal disease virus, is able to induce pores into membranes as an intermediate step of the birnavirus-penetration pathway. Using osmotic protection experiments, we demonstrate here that pep46 and its pore-forming N-terminal moiety (pep22) form pores of different diameters, 5–8 and 2–4 nm, respectively, showing that both pep46 moieties participate to pore formation. The solution structures of pep46, pep22, and pep24 (the pep46 C-terminal moiety) in different hydrophobic environments and micelles determined by ^{1}H NMR studies provide structural insights of the pep46 domain interaction. In $CDCl_3/CD_3OH$ mixture and in dodecylphosphocholine micelles, the N-terminal domain of pep46 is structured in a long kinked helix, although the C terminus is structured in one or two helices depending upon the solvents used. We also show that the folding and the proline isomerization status of pep46 depend on the type of hydrophobic environment. NMR spectroscopy with labeled phospholipid micelles, differential scanning calorimetry, and plasmon waveguide resonance studies show the peptides lie parallel to the lipid-water interface, perturbing the fatty acid chain packing. All these data lead to a model in which the two domains of pep46 interact with the membrane to form pores.

Viruses developed different strategies to deliver their genome into the host cells. Enveloped viruses possess viral proteins that promote fusion of the viral and cellular membranes (1). In contrast, nonenveloped viruses destabilize cellular membrane by mechanisms that are not yet well understood. The role of membrane lytic peptides in the entry process has been well established for different virus families. Peptides are generated by autocatalytic cleavage of a precursor such as in the case of the nodavirus γ peptide (2, 3), the poliovirus VP4 (4), and μ1C from reovirus (2, 3, 5, 6), by trypsin cleavage such in the case of rotavirus VP4 (7, 8), and by cellular proteolysis such as in the case of adenovirus protein VI (9) or by viral proteolysis such as in the case of birnavirus pVP2 generating pep46 and additional peptides (10).

Birnaviruses belong to the nonenveloped double-stranded RNA viruses. Some of them are economically important, such as the infectious bursal disease virus (IBDV),[2] which is the responsible agent of a highly contagious disease of young chickens, and the aquatic birnaviruses, the most wide spread pathogens of aquatic animals. As for other double-stranded RNA viruses, their genome must be hidden throughout the virus cycle to avoid degradation by cell defense mechanisms. Consequently, during cell entry, the birnavirus particle or at least a large molecular transcription complex has to cross the target membrane to reach the cytoplasm.

To carry out virus penetration into the cell, most double-stranded RNA viruses, such as those belonging to the Reoviridae family, exhibit a capsid harboring several concentric protein shells. The most external shell is generally lost during the entry process and is assumed to ensure a local destabilization of the target membrane (11, 12). The remaining inner shell constitutes the viral transcription machinery (13, 14). In contrast to the viruses belonging to the Reoviridae family, birnaviruses possess a single-layered capsid competent for membrane translocation (15, 16).

The major components of the birnavirus particle derive from the autoproteolytic processing of the polyprotein pVP2-VP4-

* This work was supported by a grant of the Action Concertée Incitative (ACI) "Microbiologie" from the French Ministère de la Recherche et Technologie (MRT) and the Agence Nationale de la Recherche "Projets blancs" programs.

[S] The on-line version of this article (available at http://www.jbc.org) contains supplemental Figs. S1–S9 and Table S1.

Coordinates of pep46 have been deposited at the Biological Magnetic Resonance Bank entry number 16489.

[1] To whom correspondence should be addressed. Tel.: 33-1-69-82-37-64; Fax: 33-1-69-82-37-84; E-mail: nelly.morellet@icsn.cnrs-gif.fr.

[2] The abbreviations used are: IBDV, infectious bursal disease virus; DPC, dodecylphosphocholine; PEG, polyethylene glycol; DMPC, dimyristoylphosphatidylcholine; DMPG, dimyristoylphosphatidylglycerol; DSC, differential scanning calorimetry; MLV, multilamellar vesicle; NOE, nuclear Overhauser effect spectroscopy; NOESY, NOE spectroscopy; PWR, plasmon wave guide resonance; P/L, peptide/lipid; r.m.s.d., root mean square deviation.

VP3 encoded by one of the two genomic segments (segment A). VP4 is a protease that cleaves its own N and C termini in the polyprotein, thus releasing pVP2 and VP3 (17). The sequential maturation of pVP2 takes place only upon virus particle assembly and generates VP2 and the peptides pep46, pep7a, pep7b, and pep11 (46, 7, 7, and 11 residues long, respectively) (18). The structures of IBDV and of its capsid protein VP2 were determined by x-ray crystallography (19). Fitting the atomic model of VP2 into the virion electron density map revealed that VP2 is the only component of the virus to follow the icosahedral symmetry. Although the four peptides (pep46, pep7a, pep7b, and pep11) were not visualized in the IBDV particle by x-ray crystallography (19), they are accessible to mild trypsin digestion or to biotinylation, demonstrating their close proximity to the virus surface (20).

Although pep7a, pep7b, and pep11 were shown to be inactive on membranes, pep46 has a strong activity. It interacts with liposomes and destabilizes the target cell membrane. Consequently, it has been proposed that pep46 plays a role in the cell entry process of the virus particle (18). The first 15 residues constituting the N-terminal domain of pep46 show an amphipathic character with positively charged and hydrophobic residues, similarly to some other membrane-active peptides found in nonenveloped viruses such as the γ peptide of nodavirus (21), the N terminus of VP1 of poliovirus (22), the N terminus of protein VI of adenovirus (23), and antimicrobial peptides such as melittin (24) and magainin (25). pep22, the N-terminal moiety of pep46 (22 first residues), was shown to conserve the membrane destabilization function of pep46, and residue Pro-16 was demonstrated to play a critical role in this function (18). pep46 and its N-terminal domain pep22 are able to form pores in membranes with a diameter always found to be less than 10 nm (18).

In this study, we measure the membrane pore size formed by pep22 and pep46 using osmotic protectants such as polyethylene glycols (PEG). To understand how these peptides act on the membrane, we determined by NMR experiments the structures of pep46 and its two N-and C-terminally derived domains, pep22 and pep24, respectively, in a hydrophobic solvent mixture, as well as in association with a micelle detergent that mimics the membrane environment. The orientation of pep46 and pep22 relative to the dodecylphosphocholine (DPC) micellar surface was probed by the effects of paramagnetic agents, such as the spin-labeled 5- and 16-doxyl-stearic acids and Mn^{2+}, on the NMR resonances of the peptides. Additionally, differential scanning calorimetry (DSC) and plasmon waveguide resonance (PWR) were employed to monitor the interaction of pep46 with lipids and its affinity and orientation in respect to the lipid surface. We show that pep46 is almost totally buried inside the micelle with a parallel orientation relative to the micelle surface. Our results allow us to propose a model for the membrane destabilization by pep46.

EXPERIMENTAL PROCEDURES

Peptide Synthesis—pep46 and pep22 were synthesized by automated solid phase synthesis, using the *N*-(9-fluorenyl)methoxycarbonyl strategy, and purified by reverse phase high pressure liquid chromatography using procedures already reported for the production of other proteins (26). During pep22 synthesis, 22 labeled amino acids (95%, ^{15}N and 15% ^{13}C) were incorporated. pep24 and pep22 were also purchased from Epytop (Nîmes, France) and were biotinylated at their N terminus. The sequences of the peptides derived from pep46 are described Fig. 1.

Inhibition of Hemolysis by Osmotic Protection—Immediately before use, 50 μl of sheep erythrocytes were washed repeatedly in phosphate-buffered saline and centrifuged at 3000 rpm for 5 min. Erythrocytes were resuspended in 200 μl of phosphate-buffered saline and incubated with or without 10 μM pep22 or pep46 in the presence of PEGs of different sizes for 1 h at 37 °C. The PEG concentrations were either 30 mM (27) or equivalent to about 100 mosmol. The osmotic pressure of PEGs was first estimated from the data of Reid and Rand (28), taking into account the peculiar particularity of high molecular weight PEGs and then measured with a cryoscopic osmometer (Roebling Messtechnik). Experiments at constant PEG osmotic pressure were carried out at 100 mosmol, the mean value of the osmotic pressures corresponding to 30 mM PEG concentrations. All PEGs were dissolved in phosphate-buffered saline. Similar results were obtained when the PEG osmolarity was lowered to 40 mosmol, the osmolarity of the hemoglobin in the erythrocyte (29) and the all total osmolarity adjusted to 300 mosmol with Tris-buffered saline. Preparations were then centrifuged at 3000 rpm for 3 min to pellet cells and the absorbance of supernatant at 405 nm (A_{405}) was measured in a microplate reader (EL800, Bio-Tek). Percentage of peptide-induced hemolysis was calculated as $((A_{405}\,(\text{sample}) - A_{405}\,(\text{blank}))/(A_{405}\,(\text{peptide without PEG}) - A_{405}\,(\text{blank}))) \times 100\%$, where the blank contained all components except pep22 or pep46 and PEG.

Sample Preparation and NMR Spectroscopy—The pep46, pep22, and pep24 peptides were dissolved at pH 3.5, and at pH 6.5 only for pep22 and pep24, in pure H_2O. As these peptides were shown to interact with membrane, DPC (10–100 mM) was added to the aqueous solutions (SDS, Peypin, France). In the presence of DPC, pep22 and pep24 were dissolved at pH 6.0 and pep46 at pH 3.5 and 6.2. The pH was checked and adjusted after each addition of DPC, using a small amount of NaOH and HCl. The peptides were also studied in a mixture of $CD_3OH/CDCl_3$ (1:1). In all cases, the final concentrations were about 1 mM. Two-dimensional phase-sensitive ^1H Clean-TOCSY (30) with a 70-ms spin lock, and 100- and 200-ms mixing time NOESY experiments (31), were recorded at 293, 303, 313, and 333 K on a AVANCE Bruker spectrometer operating at 600.14 MHz without sample spinning with 2K real points in *t*2, with a spectral width of 6000 Hz and 512 *t*1-increments. Pulsed-field gradients (32) were used for water suppression by a WATERGATE pulse sequence. The data were processed using XWINNMR software (Bruker). A π/6 phase-shifted sine bell window function was applied prior to Fourier transformation in both dimensions (*t*1 and *t*2). ^1H-^{15}N heteronuclear single quantum coherence experiments were performed on the pep22 sample at 1.0 mM, pH 6.5 in DPC at 293 K. The GARP sequence was used for decoupling during acquisition. Experiments were recorded on the phase-sensitive mode using echo/anti-echo gradient selection and trim pulses in inept transfer. A total of 256 FIDs of

eight scans were collected for each experiment. A $\pi/2$ phase-shifted sine square bell window function was applied prior to Fourier transformation in both dimensions ($t1$ and $t2$). The temperature was externally controlled using special temperature control system (BCU 05 Bruker). Solvent accessibility of the amide backbone signals was determined by proton/deuterium exchange studies. Samples were prepared by dissolving the lyophilized protein sample in DPC into ^2H_2O. We monitored the disappearance of the NH peaks as a function of time, by two-dimensional NOESY spectra.

NMR Structure of pep46, pep22, and pep24—NOE cross-peak volumes measured on NOESY spectrum recorded for pep46 in solution in $CD_3OH/CDCl_3$ (1:1), and in aqueous solution in the presence of 100 mM DPC for pep46, pep22, and pep24, were converted into distances, semi-quantitatively, by counting contour levels. Using the Tyr-2,6H geminal, and Asp-Hβ protons as calibration peak, NOEs signals were classified into five categories with upper distance limits ranging 2.5–5 Å. Pseudoatom corrections were added when necessary. Standard protocols using distance geometry and simulated annealing were performed in X-PLOR 3.84 (33, 34) on an SGI O_2 R12000 computer.

Peptide Location in Micelles—For locating pep46 and pep22 relative to the micelle surface, we used three different paramagnetic agents as follows: $MnCl_2$ (0.1:1 to 1.5:1 Mn^{2+}/pep22 and 0.1:1 to 5:1 Mn^{2+}/pep46), 5-doxyl stearic acid (0.3:1 to 6:1 5-doxyl/pep22 and 0.3:1 to 6:1 5-doxyl stearic acid/pep46), and 16-doxyl stearic acid (0.3:1 to 3:1 16-doxyl/pep22 and 0.3:1 to 1.5:1 16-doxyl stearic acid/pep46) (35). The effects of the spin labels were observed by comparing the peak volume intensities in ^1H-^{15}N heteronuclear single quantum coherence for pep22 and in NOESY spectra (35, 36) for pep46 labeled with unlabeled samples. The amplitude of the spectra in the presence of the three paramagnetic labels was normalized to the least affected cross-peaks.

Study of the Interaction of pep46 with DMPC and DMPG Micelles by DSC—Lipid film preparation was made by dissolving the appropriate amount of lipid (DMPC or DMPG, Genzyme) in a mixture of $CHCl_3$ and CH_3OH, 2:1 (v/v), followed by solvent evaporation under nitrogen to deposit the lipid as a film on the wall of a test tube. Final traces of solvent were removed in a vacuum chamber attached to a liquid nitrogen trap for 3–4 h. Films were hydrated with 10 mM Tris, 0.1 M NaCl, 2 mM EDTA, pH 7.6 (Tris buffer) and vortexed extensively at a temperature above the phase transition temperature of the lipid to obtain MLVs with a lipid concentration of 1 mg/ml. The peptide was added after the formation of the MLVs. The calorimetry was performed on a high sensitivity differential scanning calorimeter (Calorimetry Sciences Corp.). A scan rate of 1 °C/min was used, and a delay of 10 min between sequential scans in a series was applied to allow thermal equilibration. Data analysis was performed with the fitting program CPCALC provided by CSC and plotted with Igor. P/L molar ratios of 1:100, 1:50, 1:25, and 1:10 were used in those studies. Samples containing the peptide alone, dissolved in buffer at peptide concentrations corresponding to those at the higher peptide/lipid molar ratios studied (P/L 1:10), exhibited no thermal events over the temperature range of 0–100 °C. This indicates that the peptides do not contribute to the endothermic events observed in this study, which arise solely from lipid phase transitions and their modulation upon lipid/peptide interactions. A minimum of at least three to four heating and cooling scans were performed for each analysis.

Study of the Interaction of pep46 and Orientation Relative to a Lipid Bilayer by PWR—PWR spectra were produced by resonance excitation of conduction electron oscillations (plasmons) by light from a polarized CW laser (helium-neon; wavelength of 632.8 and 543.5 nm) incident on the back surface of a thin metal film (silver) deposited on a glass prism and coated with a layer of SiO_2 (for additional information see Ref. 37). Experiments were performed on a βPWR instrument from Proterion Corp. (Piscataway, NJ) that had a spectral resolution of 1 mdeg. The sample to be analyzed (a lipid bilayer membrane) was immobilized on the resonator surface and placed in contact with an aqueous medium, into which peptides can be introduced. The self-assembled lipid bilayers were formed using a solution (in butanol/squalene, 0.93:0.07, v/v) of 8 mg/ml egg phosphatidylcholine (Avanti Polar Lipids). The method used to make the lipid bilayers is based on the procedure by Mueller and Rudin (38) to make black lipid membranes across a small hole in a Teflon block. To accomplish this, a small amount of lipid solution was injected into the orifice in a Teflon block separating the silica surface of the PWR resonator from the aqueous phase. Spontaneous bilayer formation was initiated when the sample compartment was filled with aqueous buffer solution (37). The molecules (such as lipids and peptides) deposited onto the surface plasmon resonator change the resonance characteristics of the plasmon formation and can thereby be detected and characterized. PWR spectra, corresponding to plots of reflected light intensity *versus* incident angle, can be excited with light whose electric vector is either parallel (s-polarization) or perpendicular (p-polarization) to the plane of the resonator surface. Spectral simulation (37) and/or graphical analysis (39) allow one to obtain information about changes in the mass density, structural asymmetry, and molecular orientation induced by bimolecular interactions occurring at the resonator surface. Here, the graphical analysis method was employed. Briefly, this method consists of deconvoluting the components of the PWR spectra that are due to changes in mass in the lipid film from those that are due to changes in structural anisotropy. Such distinction can be done based on the magnitude and direction of the PWR spectra shifts observed for the p- and s-polarized light. Thus, alterations in mass density (due to addition or subtraction of mass from the membrane) result in shifts in p- and s-polarization with the same magnitude and direction (isotropic changes), whereas structure alterations lead to anisotropic changes (shifts for p- and s-polarized light that are distinct in magnitude and direction). By plotting the spectral changes observed in the (s, p) coordinate system where mass (Δ_m) and anisotropy (Δ_{str}) axes are represented based on the PWR sensitivity factor, the contribution of mass and structural changes can be obtained (39). Each point in the mass and anisotropy axis can be expressed by changes in the original coordinates (Δp and Δs) by Equations 1 and 2,

$$\Delta_m = [(\Delta s)^2_m + (\Delta p)^2_m]^{1/2} \quad \text{(Eq. 1)}$$

$$\Delta_{str} = [(\Delta s)^2_{str} + (\Delta p)^2_{str}]^{1/2} \quad \text{(Eq. 2)}$$

The sensitivity factor (S_f), a measure of the sensitivity of the instrument for the *s*-polarized relative to *p*-polarized light ($S_f = \Delta s/\Delta p$), necessary to determine the mass and anisotropy axes has been determined, for the prism used in those experiments, to be 0.74 (46).

Affinities between the peptide and the lipids were obtained by plotting the PWR spectral changes that occur upon incremental additions of ligand to the cell. Because the PWR is mainly sensitive to the optical properties of material that is deposited on the resonator surface (when a similar emergent medium (buffer) is employed, which is the case here), there is little interference from the material that is in the bulk solution. Moreover, the amount of bound material is much smaller than the total amount of ligand present in the bulk solution, and it is assumed that the bulk material is able to freely diffuse and equilibrate with the membrane. Data fitting (GraphPad Prism) through a hyperbolic saturation curve provides the dissociation constants. It should be noted that since concomitantly with the binding process other processes such as membrane reorganization and solvation occur, the dissociation constants correspond to apparent dissociation constants.

RESULTS

Hemolysis Induced by pep46 and Its Membrane-active Domain pep22 Is Inhibited by Osmotic Protection—pep46 and pep22 (Fig. 1) perforate synthetic and biological membranes, allowing liposomes and cells to release their content in the medium. Leakage occurs either through large pores directly formed by the peptides or by osmolysis after the peptides formed small pores that semi-permeabilize the membrane. To discern between these two possible mechanisms and to estimate the size of the pores induced by pep46 and pep22, we assessed the hemolysis protection by PEGs of different molecular size (37–39) in the presence of pep46 and pep22 (Fig. 2). Hemolysis protection by PEGs was carried out either at constant concentration (30 mM) (Fig. 2*A*) or at constant osmotic pressure (100 mosmol) (Fig. 2*B*). Similar results were obtained with the two procedures. High molecular weight PEGs do inhibit the release of hemoglobin from erythrocytes in the presence of pep46 and pep22. pep46 and pep22 form small pores, having characteristic diameters. For pep46, only the 6000-PEG and the 8000-PEG partially inhibited the hemoglobin release (Fig. 2, *A* and *B*). 6000- and 8000-PEG have estimated hydrodynamic diameters of 5.0 and 7.6 nm, respectively (41, 42), suggesting a diameter in the range 5–8 nm for the pores formed by pep46. For pep22, whereas the largest PEGs tested (4000, 6000, and 8000) strongly inhibited hemoglobin release, the smallest PEGs (1000 and 2000) had little effect. In these experiments, most of the protection selectivity occurred for PEGs of molecular weight in the range 2000–4000 (Fig. 2, *A* and *B*). The hydrodynamic diameter of these molecules has been estimated to about 2.5 and 3.8 nm, respectively (41, 42), suggesting a diameter in the 2–4-nm range for pores formed by pep22. Although pore diameter measurements using hemolysis protection by polyethylene glycols are not accurate (40), these results suggest that pep46 forms larger pores than pep22 and that both N- and C-terminal domains of pep46 participate in the pore formation.

Peptides	Sequence
	1 5 10 15 20 25 30 35 40 45
Pep46	FGFKDIIRAIRRIAVPVVSTLFPPAAPLAHAIGEGVDYLLGDEAQA
Pep22	FGFKDIIRAIRRIAVPVVSTLF
Pep24	PPAAPLAHAIGEGVDYLLGDEAQA

FIGURE 1. **Primary sequence of the peptide pep46 and of the two peptides deriving from its N- or C-terminal domains (pep22 and pep24).**

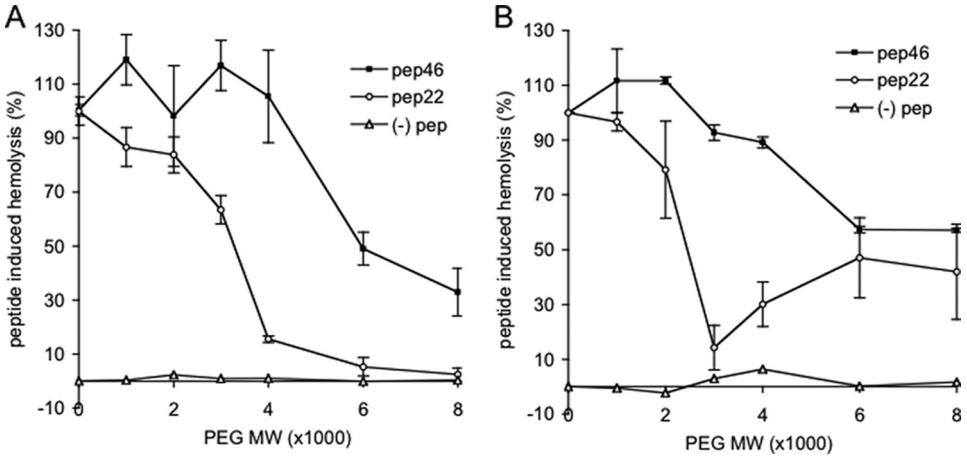

FIGURE 2. **Inhibition of peptide-induced hemolysis by osmotic protection.** Hemolysis reactions were performed with or without 10 μM pep46 or pep22 in the presence of polyethylene glycols of different sizes. For both cases, PEGs were added at a concentration of 30 mM (*A*) or at a concentration equivalent to 100 mosmol (*B*). In the absence of peptide, no hemolysis is observed in constant PEG concentration (30 mM (−) pep (*A*)) or constant PEG osmolarity (100 mosmol (−) pep (*B*)) conditions. Each experimental points and *error bar* are the mean ± S.D. of four independent experiments.

NMR Studies of pep46 and Derived Peptides (pep22 and pep24) in Micelles—pep46 was found soluble in pure water at pH 3.5, but not structured (supplemental Fig. S1*A*), and insoluble at a more biological pH, such as 6.0. DPC was chosen to study pep46 and derivates since it contains a zwitterionic headgroup, which is a proper cell membrane lipid mimetic. It is also a relatively small molecule, which facilitates NMR studies (41, 42) by solubilizing efficiently hydrophobic or amphipathic α-helices (36). pep46 was dissolved in the presence of 10 mM DPC, at pH 3.5, and increasing amounts of DPC were added until no modification was observed on the one-dimensional spectra, which indicates the stabilization of the pep46 structure in micelles. Until 50 mM, DPC increments induced chemical shift variations and, surprisingly, led to a decrease in the line width of ^{1}H resonances (for comparison see supplemental Fig. S1, *B* and *C*). Between 50 and 100 mM DPC, the spectra were almost identical (supplemental Fig. S1, *C* and *D*). Similar folding variations have been observed by CD for pep46, in the function of DPC concentration. Indeed, until 50 eq of DPC, changes in CD spectra are observed, and between 50 and 100

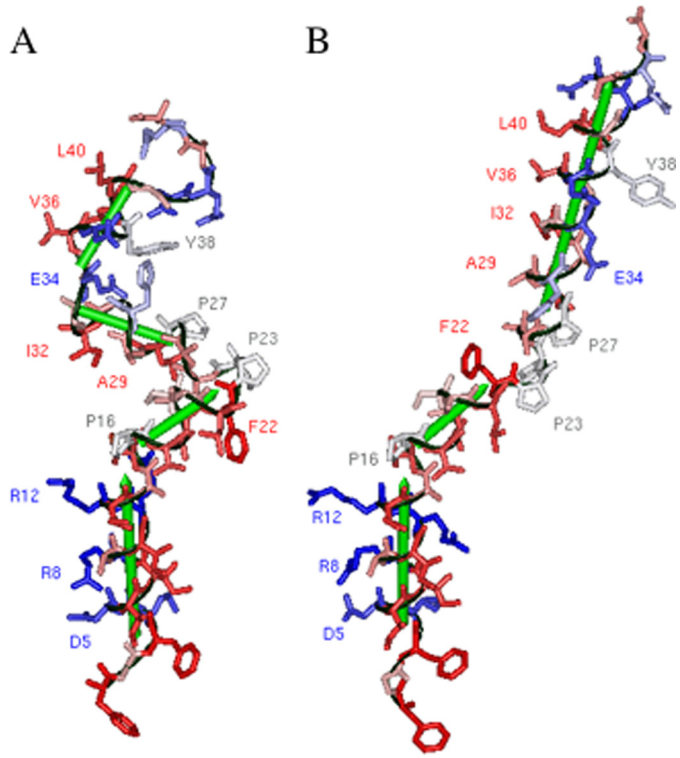

FIGURE 3. **Comparison of the pep46 structures obtained in presence of DPC (*A*) and $CD_3OH/CDCl_3$ (1:1) (*B*).** The helices are represented as *green cylinders*, and the residues are colored according to their hydrophobicity (*red,* hydrophobic residues; *blue,* hydrophilic residues).

eq of DPC, the spectra are almost identical (supplemental Fig. S2). In the presence of DPC, pep46 is also soluble at a more biological pH value, such as 6.2. Unfortunately, we observed a broadening of the signals with increasing pH (supplemental Fig. S1, *D* and *E*, and Fig. S3) or in phosphate buffer, pH 6.8 (supplemental Fig. S1*F*). Nevertheless, most of the resonances in the NOESY spectra recorded at pH 6.2 were assigned by comparison with the NOESY spectra recorded at pH 3.5. Although some amide protons underwent significant chemical shift variations (supplemental Fig. S3), we confirmed that pep46 very likely adopts the same three-dimensional conformation at pH 3.5 and 6.2 because all the secondary structure medium NOEs observed at low pH have also been assigned in the NOESY spectra at pH 6.2, despite the significant increase of the line widths (supplemental Fig. S3). Moreover, we observed that the Hα chemical shift index analysis, which represents the difference between the observed chemical shift and the random coil values (43), is very similar whatever the pH values, 3.5 or 6.2 (supplemental Fig. S4). An upfield trend (*i.e.* negative secondary shift) for the Hα resonances of residues suggests that this peptide consists predominantly of helical structural elements at these two pH values. These results are confirmed by the CD spectra (supplemental Fig. S2). The increase of DPC concentration induces a structural transition of pep46 from a random coil to an α-helical structure characterized by the presence of two minima at 209 and 220 nm in the CD spectra. Similar spectra are obtained at pH 3.5 and 6 for pep46 in the presence of 100 eq of DPC, suggesting the peptide presents similar folding in these conditions.

TABLE 1
NMR restraints and structural statistics

NMR derived distance restraints		
• Total	483	
• Intraresidue	211	
• Sequential (|i-j| =1)	152	
• Medium-range (1< |i-j| ≤4)	120	
• Long-range (|i-j| >5)	0	
Distance violations (Å)		
• > 0.2	0	
r.m.s.d. (Å) from experimental		
• distance restraints	(514) 0.027 ± 0.004	
r.m.s.d. from idealized geometry		
• bonds (Å)	(715) 0.0048 ± 0.0002	
• angles (deg)	(1299) 0.66 ± 0.01	
• improper angles (deg)	(45) 0.45 ± 0.02	
Xplor potential energies (Kcal/mol)		
• E_{NOE}	20.8 ±6.0	
• E_{VDW}	-189.9 ± 6.6	
• E_{BOND}	13.1 ±1.4	
• E_{ANGLES}	86.8 ±2.0	
• $E_{IMPROPERS}$	11.5 ± 0.8	
• E_{TOTAL}	-1767.8 ± 45.2	
Ramachandran analysis of residues		
• favored region (%)	90.7	
• additional allowed regions (%)	7.6	
• generously allowed regions (%)	1.4	
• disallowed regions (%)	0.2	
Atomic rms deviation to mean structure (Å)	**Backbone atoms**	**Heavy atoms**
(3-15)	0.26 ± 0.12	1.75 ± 0.63
(17-22)	0.66 ± 0.38	1.29 ± 0.53
(3-22)	0.70 ± 0.29	1.80 ± 0.52
(18-27)	0.91 ± 0.43	1.05 ± 0.51
(27-41)	0.33 ± 0.16	1.12 ± 0.41

Contrary to pep46, pep22 and pep24 are soluble in pure H_2O at pH 6.0, but no characteristic NOEs of any secondary structure were found in these conditions. DPC increments did not induce a decrease in the line width of these two peptides, but as for pep46, we observed chemical shift variations, characteristic of the secondary structure formations. Only *trans*-proline conformers were observed in presence of DPC. The structures of pep22 and pep24 were calculated using the NMR restraints collected for the peptides in 100 mM DPC at pH 6.0. The pH has no effect on the line widths of these two shorter peptides. pep22 adopts a similar conformation to its corresponding counterpart in pep46, an α-helix spanning residues Phe-3 to Phe-22. On the contrary, pep24 adopts only one α-helix instead of the two observed in the corresponding domain in pep46 (supplemental Fig. S5), arising from additional secondary structure NOE contacts involving the three glycines, Gly-33, Gly-35, and Gly-41, a residue known to often provide flexibility in the protein structure (supplemental Table S1). The *cis/trans* isomerism of Pro-16 and Pro-23 noted in pep46 (18) was not observed in pep22 and pep24, respectively. Indeed, the duplication of Val-15, Val-17, and Val-18 resonances on one hand, and of Ala-25, Ala-26, and His-30 on the other hand, observed for pep46, were not detected in the NMR spectra of pep22 and pep24.

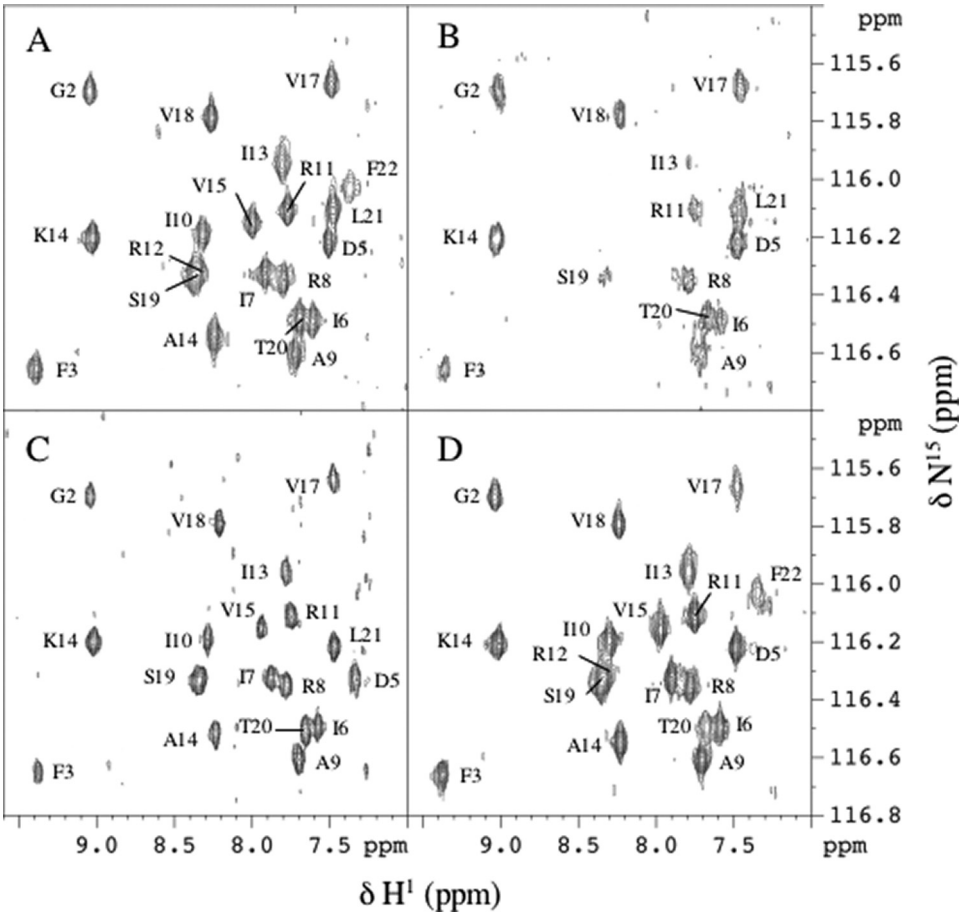

FIGURE 4. **Effect of paramagnetic agent on ^{15}N-labeled pep22 at 293 K.** *A*, ^{1}H-^{15}N heteronuclear single quantum coherence of 1 mM pep22 with 100 mM DPC (100:1 DPC/pep22 mol ratio); *B*, 100 mM DPC and 3 mM 16-doxyl stearic acid; *C*, 100 mM DPC and 6 mM 5-doxyl stearic acid; and *D*, 100 mM DPC and 3 mM $MnCl_2$. Cross-peaks are labeled using the one-letter amino acid code.

NMR Studies of pep46, pep22, and pep24 in Hydrophobic Solvent—To better characterize the potential function of the N- and C-terminal domains of pep46 in membrane destabilization, pep46 and its two derivates were studied in a mixture of solvents ($CD_3OH/CDCl_3$), shown to mimic the hydrophobicity of membranes (44–46). The complete chemical shift assignment of the backbone and side chain protons was achieved for all the amino acids of pep46 (supplemental Fig. S6). Only the sequential NOE cross-peaks, characteristic of a *trans*-conformation of prolyl bonds, were observed in NMR spectra for pep46 solubilized in $CD_3OH/CDCl_3$ (1:1). Analysis of the NOESY experiments, based on the observed medium range NOEs, reveals that pep46 is organized into two domains. Indeed, typical NOEs corresponding to a classical α-helix were found for the 3–22 and the 27–46 residues of pep46 (supplemental Figs. S7 and S8). In $CD_3OH/CDCl_3$, pep46 shows almost the same general characteristics as those obtained in DPC (Fig. 3). The structure is characterized by an N-terminal curved α-helix showing an approximate 115° angle (120° in DPC) between the two helical domains, spanning residues 3–22, followed by a loop constituted by the proline-rich region (residues 23–27), and ended by one α-helix (residues 28–41). The first helix (residues 3–22) in pep46 is perfectly well defined with an average r.m.s.d. for the 10 best structures calculated on the backbone atoms of 0.70 (± 0.29) Å (Table 1). This helix has the characteristics of an amphipathic helix in the region (residues 3–15). The amino acid side chains of Lys-4, Asp-5, Arg-8, Arg-11, and Arg-12 form its hydrophilic face, whereas the side chains of Phe-3, Ile-6, Ile-7, Ala-9, Ile-10, Ile-13, and Ala-14 provide an uninterrupted hydrophobic surface. The Pro-16 appears to induce a break in the helix (residues 3–22). The segment consisting of residues 17–22 is exclusively composed of hydrophobic residues. The C-terminal domain (residues 27–41) is better defined in $CD_3OH/CDCl_3$ than in presence of DPC, and it is characterized by one well defined long helix with an average r.m.s.d. for the backbone atoms of 0.33 (± 0.16) Å (Table 1), instead of the two helices found in DPC (18) (Fig. 3*A*). The region (residues 32–41) presents the characteristics of a short amphipathic helix, with the hydrophilic face constituted by the amino acid side chains of Glu-34, Asp-37, and Tyr-38 and the hydrophobic face composed of the side chains of Ile-32, Val-36, Leu-39, and Leu-40. Altogether, these data show that the C-terminal domain of pep46 and pep24 exhibits a structure that strongly depends on the environment.

Positioning of pep22 and pep46 in Detergent Micelles by Spin-labeled Probes and Mn^{2+}—To investigate how pep22 and pep46 form pores in membranes and to understand the contribution of the C-terminal domain of pep46 in the pore formation, we determined their orientation in DPC micelles through the analysis of the effects of 5- and 16-doxyl stearic acids and Mn^{2+} ions on the proton signals of the peptides in micelles. Although manganese ions were used to probe the residues exposed to the solvent close to the micelle surface, both 5-doxyl stearic acid and 16-doxyl stearic acid were used for identification of the membrane-embedded residues (47). The 16-doxyl spin label is located in the center of DPC micelles, whereas the 5-doxyl stearic spin label is positioned near the phosphate moiety, below the headgroup (47).

Positioning of pep22—The effect of paramagnetic probes was estimated from ^{1}H-^{15}N heteronuclear single quantum coherence experiments by comparing the spectra with and without 5- or 16-doxyl stearic acid and Mn^{2+} (Fig. 4). With a 16-doxyl stearic acid/pep22 ratio of 3:1, the resonances of Ile-10, Ala-14, and Val-15 disappeared, and those corresponding to residues located on both sides of these amino acids (Phe-3, Ile-6, Ile-7, Arg-11, Arg-12, Ile-13, Ser-19, and Phe-22) were considerably reduced (Figs. 4*B* and 5*A*). The overall effects of 5-doxyl stearic

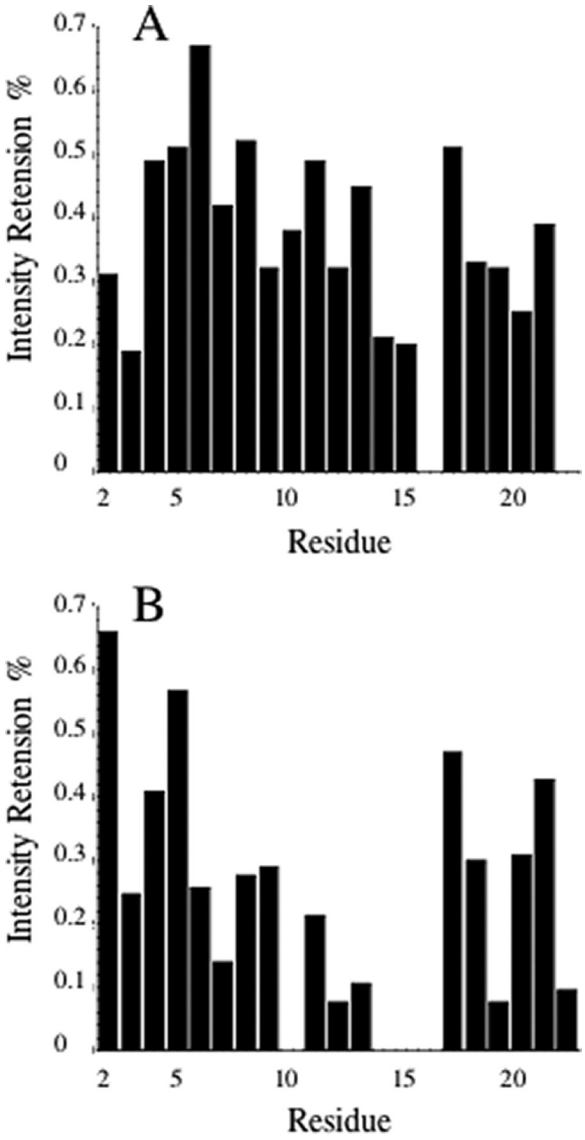

FIGURE 5. **Paramagnetic quenching obtained for pep22 in DPC micelles using 5- and 16-doxyl stearic acid.** Intensity retention plot is shown for pep22 in the presence of 3 mM 16-doxyl stearic acid (*A*) and 6 mM 5-doxyl stearic acid (*B*).

acid/pep22 ratio of 6:1 on pep22 were smaller and caused the greatest reduction of the Phe-3, Ala-14, and Val-15 resonances and to a lesser extent of Gly-2, Ala-9, Ile-10, Arg-12, Val-18, and Ser-19 (Figs. 4*C* and 5*B*). There was a noticeable periodicity in the resonance intensity decrease around the helix because the hydrophobic face of the helix, including the Phe-3, Ile-6, Ile-7, Ile-10, Ile-13, and Ala-14 residues, is the least accessible and mostly buried in the micelles relative to the rest of the helix. Mn^{2+} causes a reduction in the resonance intensities of Thr-20 and the disappearance of Leu-21, demonstrating that these C-terminal residues are more solvent-exposed (Fig. 4*D*). All these results suggest that pep22 is inserted inside the DPC micelles, but lying parallel to the surface, with the most quenched residues located toward the micelle core (Ile-7, Ile-10, Ala-14, Val-15, and Ser-19) or toward the polar headgroup (Arg-11, Arg-12, Ile-13, and Ser-19).

Positioning of pep46—The position of pep46 with respect to the micelle surface was estimated from the level of reduction of

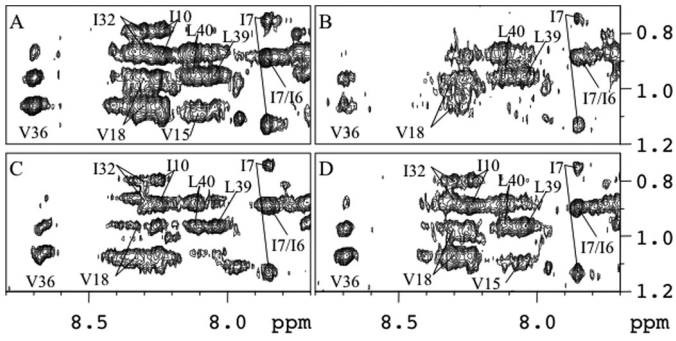

FIGURE 6. **Effects of the spin-labeled molecules 16- and 5-doxyl stearic acid and Mn^{2+} on the NOESY spectra of pep46 in 100 mM DPC micelles.** *A*, NH-aliphatic region of a NOESY spectrum of pep46, recorded with a mixing time of 200 ms, at 323 K and pH 3.5. Corresponding regions with 16 doxyl stearic acid (*B*), 5-doxyl stearic acid (*C*), and $MnCl_2$ (*D*) are represented.

TABLE 2

Effects of the spin labels on the residues of pep46

Semiquantitative classification according to the following abbreviations: L, low effect; M, moderate effect; S, strong effect. The exchange of labile protons in pep46 when bound to DPC micelles was studied by adding D_2O to a lyophilized sample. The exchangeable protons of residues Ile-6, Arg-8, Ala-9, Arg-11, Arg-12, Ala-14, Val-15, Val-17, Val-18, Ser-19, Thr-20, His-30, Ile-32, Gly-33, Gly-35, Val-36, Tyr-38, and Leu-40 are still present in the NOESY spectrum recorded after 8 h (○); the Ile-39 amide proton in still present after 24 h (●), Ile-13 after 32 h (●), and Ile-7 and Ile-10 after 64 h (●).

	Hbond	16-DOXYL stearic acid			5-DOXYL stearic acid			$MnCl_2$				Hbond	16-DOXYL stearic acid			5-DOXYL stearic acid			$MnCl_2$		
		L	M	S	L	M	S	L	M	S			L	M	S	L	M	S	L	M	S
Phe 1		L				M					Pro 24			M				S			
Gly 2							S				Ala 25		L					S			
Phe 3			M				S				Ala 26		L				M				
Lys 4		L				M					Pro 27		L				M				
Asp 5		L				M					Leu 28			M				S			
Ile 6	○			S		M					Ala 29			M				S			
Ile 7	●			S		M					His 30	○	L				M				
Arg 8	○					M					Ala 31		L				M				
Ala 9	○		M			M					Ile 32	○			S		M				
Ile 10	●			S		M					Gly 33	○			S			S			
Arg 11	○		M				S				Glu 34						M				
Arg 12	○	L					S				Gly 35	○		M				S			
Ile 13	●			S		M					Val 36	○			S		M				
Ala 14	○			S			S				Asp 37						M		L		
Val 15	○			S			S				Tyr 38	○					M		L		
Pro 16		L				M					Leu 39	●		M				S			
Val 17	○			S			S				Leu 40	○		M				S			
Val 18	○			S			S				Gly 41						M		L		
Ser 19	○	L					S				Asp 42						M		L		
Thr 20	○	L				M					Glu 43						M		L		
Leu 21			M				S				Ala 44							S	L		
Phe 22				S			S				Gln 45							S	L		
Pro 23		L				M					Ala 46							S	L		

the backbone and side chain cross-peak intensities in ^1H NOESY (Fig. 6). The influence of each of the three paramagnetic probes on the 1–15-residue domain of pep46 is almost the same as that observed on pep22, because the 16-doxyl stearic acid caused the same periodic medium or strong reduction of cross-peak intensities on the hydrophobic residues (Phe-3, Ile-6, Ile-7, Ala-9, Ile-10, Ile-13, Ala-14, and Val-15), and the 5-doxyl stearic acid on the five first N-terminal residues and on the positively charged arginines 8, 11, and 12 (Table 2). The effects of the three paramagnetic probes are mapped onto one of the pep46 structures (Fig. 7*A*). The results showed that the 3–15-residue helical domain probably lies parallel to the micelle surface, with the hydrophobic face toward the interior of the micelle, and the positively charged residues (Arg-8, Arg-11, and Arg-12) interacting with the negatively charged phosphate headgroups, anchoring the peptide just below the micelle surface (Fig. 7*B*).

In contrast, strong differences were observed on the 17–22-residue domain within pep22 and pep46. Although the reso-

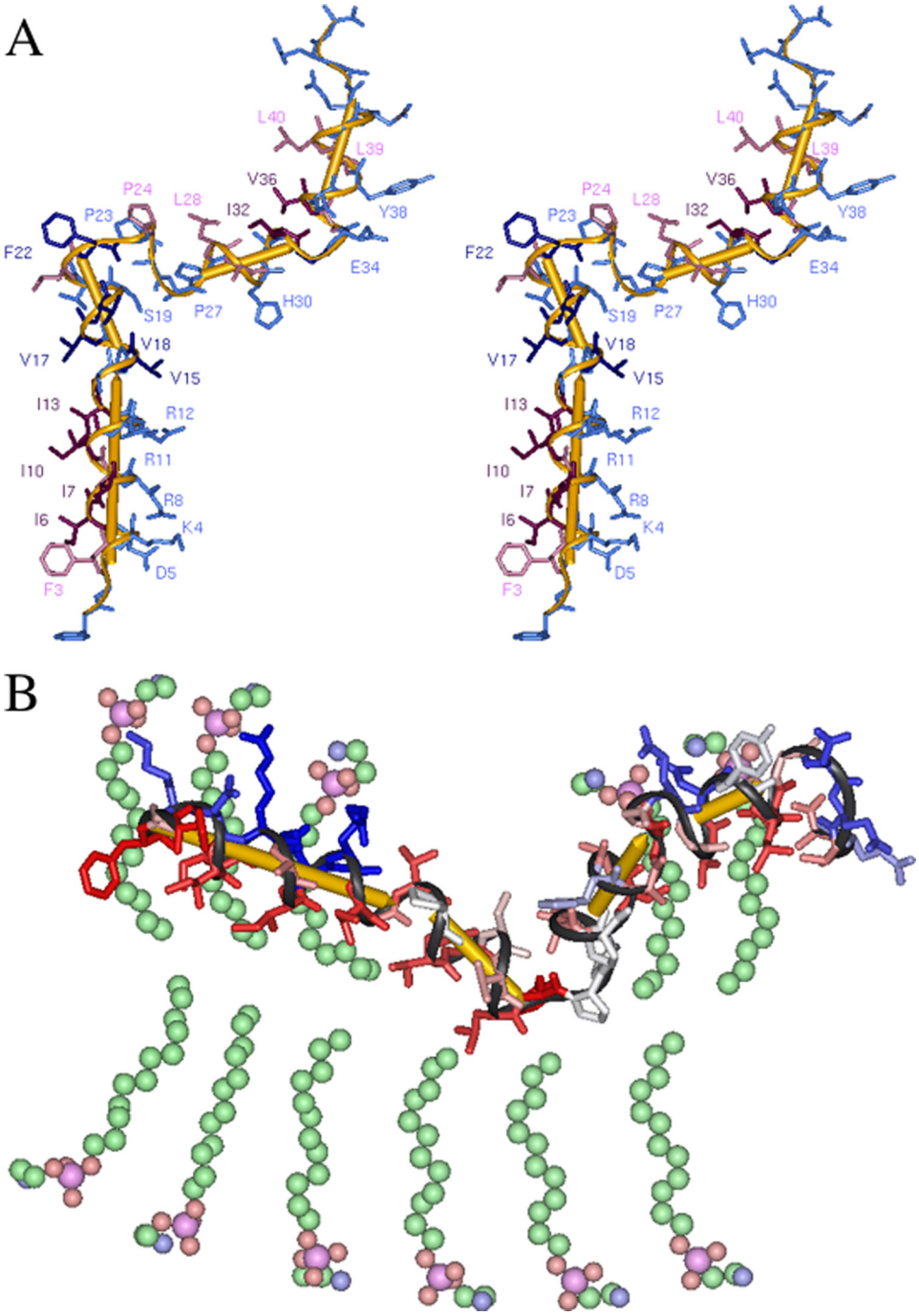

FIGURE 7. *A,* stereoview of one of the pep46 structures obtained in presence of DPC. The signal reductions greater than 50% are mapped onto the pep46 structure. Residues that are the most affected upon addition of 16-doxyl stearic acid are colored *dark purple*. Residues that are quenched by the addition of 5-doxyl stearic acid are colored *light blue*. Residues that at the same time are strongly quenched by the 5-doxyl stearic acid and 16-doxyl stearic acid are colored *dark blue*. Residues that are affected strongly by 5-doxyl stearic acid and moderately by 16-doxyl stearic acid are colored *light purple*. *B,* schematic representation of the interaction of pep46 DPC micelle. One representative structure of pep46 is positioned with the basic residues interacting with the negatively charged phosphate headgroup of DPC and the hydrophobic residues plunging into the fatty acid chains of the lipid.

nance intensities of Val-17, Leu-21, and Phe-22 are clearly influenced by Mn^{2+} in pep22 (Fig. 4*D*), in pep46 these same residues did not show significant reduction in their resonance intensities upon addition of this paramagnetic probe (Table 2). Residues 17–22 of pep46 are more buried into the lipid micelle than the corresponding ones of pep22. A significant periodic reduction in the cross-peak intensities of Ala-14, Val-15, Val-17, Val-18, Leu-21, and Phe-22 was observed in presence of both the 16-doxyl and the 5-doxyl stearic acid (Table 2), although a significant reduction in the intensity of the cross-peaks was observed only in presence of 5-doxyl for the following residues: Pro-16, Ser-19, Thr-20, Pro-23, Ala-25, Ala-26, and Pro-27. These residues are located on the same side of the structure (supplemental Fig. S9).

A periodicity in the remaining amplitude *versus* the residue number was also apparent in the C-terminal segment of 28–40 residues (Fig. 7*A* and Table 2). The most affected residues under the 16-doxyl stearic acid effect are Ile-32 and Val-36, whose side chains interact with the lipid acyl chains and penetrate deeper into the micelle. The 5-doxyl stearic acid probe caused the largest changes in Leu-28, Ala-29, Gly-33 and Gly-35, Leu-39, Leu-40 and to a lesser degree in His-30, Ala-31, Glu-34, Asp-37, and Tyr-38. Therefore, these residues are buried into the lipid acyl chain region near the headgroup region. Leu-28, Ala-29, Ile-32, Val-36, Leu-39, and Leu-40 on one hand and His-30, Glu-34, Asp-37, and Tyr-38 on the other hand are located, respectively, on the hydrophobic and hydrophilic faces of the C-terminal helix (Fig. 3*A*). This part of the protein also appears to be inserted in the micelle, although to a lesser extent when compared with the first N-terminal helix, with a parallel orientation relative to the lipid surface. Only the residues of the C-terminal part of pep46 underwent attenuation, although low, of their cross-peaks in the presence of Mn^{2+} (Table 2). These results are corroborated by the amide exchange experiments. We solubilized the protein-micelle complex in D_2O. Slowly exchanging protons were detected by NOESY spectra acquired every 8 h for a period of 64 h. The most solvent-protected amino acids were observed in the regions, including residues 6–20 on the one hand, and residues 30–40 on the other hand (Table 2).

Effect of pep46 on DMPC and DMPG Lipid Phase Transition—The degree of interaction of pep46 with lipids was monitored by following the changes in the lipid phase pre-transition arising from the conversion of the lipid phase structure L_β' to P_β' and the main phase transition corresponding to the conversion from P_β' to L_α (T_m) upon peptide/lipid interaction. In this study, the peptide was added to the lipid after MLV formation to better mimic the biological system. The lipids employed in this study are the DMPC and DMPG (48–50). These lipids have often been used in DSC studies as they possess a highly energetic phase transition that occurs at room temperature. DMPC constitutes a good model of eukaryotic cell membranes. Moreover, this zwitterionic lipid resembles DPC used here in the NMR studies. Because electrostatic interactions between peptides and lipids have been shown to play an important role and because eukaryotic cells possess some charged lipids, the anionic lipid DMPG was also used in these studies. In terms of the lipid model, MLVs were chosen because they produce sharp and energetic phase transitions and have been routinely used in DSC studies. The interaction of pep46 with the lipids clearly affects the thermotropic lipid behavior with either a great decrease (in the case of DMPC) or abolishment of the pre-transition (DMPG), at P/L of 1:10) (Fig. 8 and Table 3). The pre-transition, which is observed in some saturated lipids, is due to the tilting of the hydrocarbon side chains and is sensitive to the presence of interacting molecules. The untilting of the hydrocarbon chains by pep46 may be explained by a simple neutralization of the headgroup charge by the cationic peptide, which will result in reduced electrostatic headgroup repulsion and concomitantly in a smaller headgroup area observed in the case of DMPG. Moreover, the cooperativity and the enthalpy of the main phase transition were also affected by the peptide. The enthalpy of the main phase transition is mainly due to the disruption of van der Waals interactions between the fatty acid chains, and perturbations on this transition are indicative of intercalation of the peptide between the fatty acid chains. This indicates a strong interaction of pep46 with the lipids not only at the level of the headgroup but with an intercalation in between the fatty acid chains.

Interaction of pep46 with Egg Phosphocholine Lipid Bilayers Studied by PWR—This technique was used to directly monitor the interaction of pep46 with the lipid bilayer and the changes induced by the peptide lipid bilayer organization and total mass (37). PWR spectral changes occurring after addition of pep46 to the PWR cell compartment containing an egg phosphocholine bilayer are shown in Fig. 9, *A* and *B*. The binding of pep46 to the bilayer leads to a decrease in the resonance angle position for both *p*- and *s*-polarizations and to changes in the spectral depth. To characterize the mass and the structural changes that accompany the interaction of the peptide with the lipid bilayer (for details see Ref. 39), we performed a graphical analysis, which, by plotting the data points on an *s*, *p*-coordinate system containing both mass and structural axis placed according to the sensitivity factor of the PWR sensor, allows the determination of the mass and structural anisotropy contributions to the process. Thus, the origin of the plot corresponds to the lipid bilayer in the absence of ligand, and the data points shown correspond to the shifts induced by peptide binding to the bilayer. The binding of pep46 to the lipid bilayer produced very large spectral changes (about −30 mdeg for *p*-polarized light and about −53 mdeg for *s*-polarized light), which corresponds in magnitude to about 1/3 to 1/4 of that obtained upon the formation of the lipid bilayer. Such large spectral changes indicate that the peptide induces large structural and mass changes in the lipid bilayer. Indeed, the graphical analysis indicates an ~70% change is mass (decrease) *versus* ~30% change in structure. A decrease in mass density results mainly from a decrease in the mass of the lipid bilayer due to removal of lipid from the bilayer accompanied by lipid structural rearrangements. Addi-

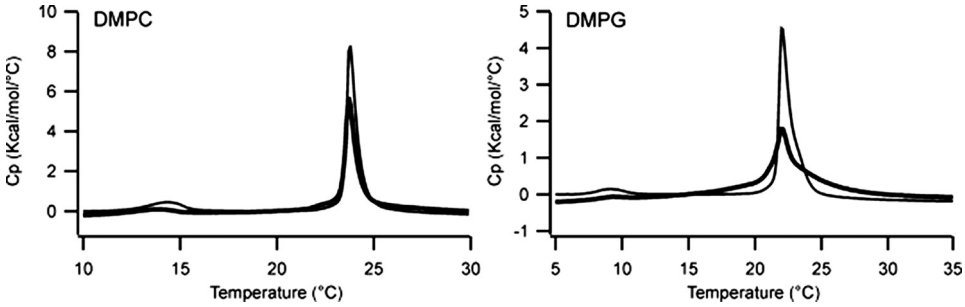

FIGURE 8. **High sensitivity DSC heating scans illustrating the effect of the addition of pep46 (*bold lines*) on the thermotropic phase behavior of DMPC and DMPG at a P/L 1:25.** Thermodynamic parameters are given in Table 3.

TABLE 3

Thermodynamic parameters for the DMPC and DMPG phase transition in the absence and presence of peptide pep46 at different P/L molar ratios

Pre-transition is L_β' to the P_β', and main transition is P′ to L_α.

P/L	*T* pre-transition	Δ*H* pre-transition	Δ*S* pre-transition	T_m	Δ*H* main transition	Δ*S* main transition
		kcal/mol	*kcal/mol*		*kcal/mol*	*kcal/mol*
DMPC alone	14.4	1.1	0.004	23.8	6.7	0.022
1:100	14	1.1	0.004	23.7	7.2	0.024
1:50	14	0.9	0.003	23.7	6.5	0.022
1:25	13.8	0.6	0.002	23.7	5.6	0.019
1:10	13.8	0.3	0.001	23.7	4.0	0.014
DMPG alone	9.1	0.4	0.001	22	6.1	0.021
1:100	9.3	0.4	0.002	22.1	6.6	0.022
1:50	9.2	0.4	0.001	22.1	7.5	0.025
1:25	9.2	0.1	0.001	22	5.4	0.018
1:10	Disappears	Disappears	Disappears	23.5	6.5	0.022

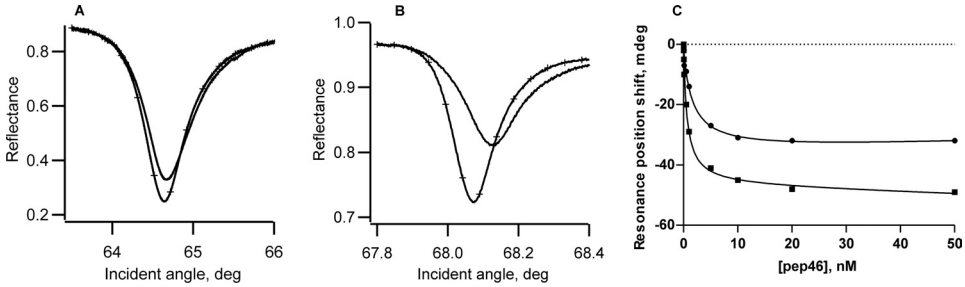

FIGURE 9. **Interaction of pep46 with an egg phosphocholine lipid bilayer monitored by PWR.** PWR spectra (*A* and *B*) obtained for the lipid bilayer (*solid line*) and after addition of pep46 to the bilayer (*solid line* with +) were obtained for *p*- and *s*-polarized light, respectively. The resonance position shifts obtained for *p*- (●) and *s* (■)-polarizations for the incremental addition of pep46 are represented and the hyperbolic binding curve from which a K_d value of 1 nM was obtained (*C*).

tionally, it should be noted that the magnitude of the resonance angle shift was much larger for *s*- than *p*-polarization, meaning that larger structural and mass changes are occurring parallel rather than perpendicular to the bilayer. This suggests an orientation of the peptide with its long axis parallel to the lipid bilayer. Regarding the affinity of pep46 to the bilayer, a K_d of about 1 nM was calculated (Fig. 9*C*). Moreover, the changes in spectral depth induced by the peptide indicate alterations in bilayer thickness.

DISCUSSION

pep46 was shown to be the central actor of the entry mechanism of birnaviruses (18). In this study, we enlighten the pore forming activity of pep46 in membranes. The diameter of the pore was estimated to be near 5–8 nm by following osmotic protection of erythrocytes from hemolysis. This value is in agreement with data obtained previously by cryo-microscopy that showed the pore diameters to be always less than 10 nm. It is worthwhile to note that pep22, the perforating domain of pep46, gives smaller pore diameter (2–4 nm). These data prove that pep24 that has no permeabilization activity cooperates with pep22 to form larger pores. The different diameters supposedly arise from different sizes or self-aggregation properties of the perforating peptides pep22 or pep46.

We combined DSC, PWR, and NMR spectroscopy studies to gain more information on pep46 structure-function relationships, in particular its position in the membrane. We show that the structures of pep46 and the two peptides derived from its N- or C-terminal extremities, pep22, and pep24, respectively, significantly depend on the solvent employed. When aqueous solution and physiological pH are used, pep22 and pep24 are soluble but are not folded, in contrast to pep46 that is only soluble at acidic pH. In more hydrophobic solution (CD_3OH/$CDCl_3$ (1:1)) or in the presence of DPC, pep46 shows similar solubility properties to pep22 and pep24. Surprisingly, we observed that increasing DPC concentration in pep46 solution induced a narrowing in the line widths of pep46 in the ^{1}H NMR spectra. This suggests that pep46 has a high tendency to aggregate. The hydrophobic environments drastically reduce intermolecular hydrophobic interactions between the accessible hydrophobic domains of pep46, allowing its complete dissolution whatever the pH. Aggregation takes place most probably through the highly hydrophobic domain located between amino acids 20 and 29 of pep46 (Fig. 3), because each N- and C-terminal domain taken separately does not aggregate in the same conditions. Moreover, the fact that pep24 acquires a secondary structure in hydrophobic environment shows that although it has no permeabilization activity it interacts with membranes.

The major difference between the structures of pep46 obtained in CD_3OH/$CDCl_3$ (1:1) and in the presence of DPC concerns its C-terminal domain, which was shown to be folded in either one α-helix (residues 28–41) or in two successive short helices (residues 28–33 and residues 35–41), respectively (Fig. 3). The structural heterogeneity observed in DPC micelles between the two C-terminal helices results from the high degree of chain flexibility at the position of two glycines (Gly-33 and Gly-35). This structure heterogeneity is not found for pep24. Indeed, a perfectly well defined α-helix involving the 27–41-residue region is observed for pep24 in DPC micelles (supplemental Fig. S5). On the contrary, the same α-helical structure is observed in pep22 and in its corresponding N-terminal domain in pep46. pep24 and its corresponding domain in pep46 do not interact in the same way with DPC micelles. This difference is probably governed by the interaction of the N-terminal domain of pep46 with DPC micelles, which constraints the conformation of its C-terminal domain. Gly-33 and Gly-35 provide the necessary flexibility in the C terminus of pep46 to undergo the conformational adaptability that favors a better orientation of the peptide relative to the membrane.

As the DPC micelles are prolate ellipsoids with a thickness comparable to that of a plasmic membrane (51), the topology of the pep22 and pep46 peptides relative to the surface and the interior of the DPC micelle was investigated using paramagnetic probes, such as Mn^{2+}, 5-doxyl stearic acid, and 16-doxyl stearic acid. Important information on the location of the peptides in the membrane can be obtained at a low protein/lipid ratio. The first 15 residues of pep22 and pep46 are buried in the micelle. Indeed, they form a helix that lies more or less parallel to the micelle surface with the hydrophobic face toward the center, and Arg-8, Arg-11, and Arg-12 anchoring this domain to the headgroup of the DPC by interactions between the arginine positively charged guanidinium groups and the negatively charged DPC phosphates (Fig. 7*B*). In the very hydrophobic domain (residues 14–22) of pep46, some residues are strongly affected by both the 5- and the 16-doxyl stearic acid such as Ala-14, Val-15, Val-17, Val-18, and Phe-22. These hydrophobic residues are located on the same side of pep46(14–22) helix and constitute a hydrophobic platform (supplemental Fig. S9). This N-terminal domain is followed by a relatively more flexible region, pep46(23–30), containing three prolines (Pro-23, Pro-24, and Pro-27). These three successive residues nevertheless impose rigid constraints on rotation about the N-Cα bond of the backbone and are responsible for the formation of a turn (Fig. 7*A*), which probably imposes the relative orientation of the N- and C-terminal domains of pep46. Although less buried inside the micelle than the first 15 residues of pep46, its C-ter-

minal domain is also parallel to the surface of the DPC micelle, but it does not insert so deeply in the lipid aliphatic chains.

The interaction of pep46 with DMPC and DMPG was monitored with DSC by following the effect of the peptide on lipid phase transitions. The results obtained with DMPC confirmed that the peptide interacts strongly with the lipid phosphate headgroups and intercalates within the fatty acid chain region as indicated by the perturbation of both the pre- and main lipid phase transitions. PWR studies indicate that the peptide has a strong affinity (K_d ~1 nM) for egg phosphocholine lipid bilayer and produces important changes both in the structure and mass of the membrane. Therefore, the decrease in mass of the lipid bilayer could be explained by either a peptide-induced efflux of lipid into the plateau Gibbs border caused by peptide intercalation between the fatty acid chains or by bilayer solubilization (with or without pore formation). In agreement with NMR data, PWR studies demonstrate that pep46 is oriented parallel to the bilayer, at least in the first stage of peptide/lipid interaction at a time the decrease in mass is not observed.

Critical residues of pep46 for virus rescue have been identified using a reverse genetic system (18). Indeed, among the 46 substitutions generated for each residue of pep46, 17 did not allow virus recovery (Phe-1, Gly-2, Lys-4, Ile-7, Ile-10, Arg-11, Ala-14, Pro-16, Ala-25, Leu-28, Ala-29, Ile-32, Gly-35, Leu-39, Leu-40, Gln-45, and Ala-46). As represented in Fig. 7*A*, the hydrophobic residues Ile-7 and Ile-10 and Leu-28, Ile-32, and Leu-39, are, respectively, located on one side of each of the N- and C-terminal helices of the peptide. These residues are located toward the hydrophobic center of the micelles. The basic residues, Lys-4 and Arg-11, are located on the same side of the N-terminal helix and are responsible for the anchoring of this domain to the polar heads (Fig. 7*B*). The results imply that the helical kink introduced by the Pro-16 residue is probably crucial for the permeabilization activity of pep46. The appearance of such kinked helix is also present in the flock house virus γ peptide (nodavirus) (21) and in some antimicrobial peptides such as gaegurin (52), maculatin (53), buforin II (54), and melittin (55).

Cryomicroscopy experiments in a previous publication (18) showed that liposomes incubated with pep46 undergo structural modifications of the thickness of the membrane leading to the formation of pores. PWR, DSC studies, and NMR data are in good agreement with these results and suggest that electrostatic attractions provided by DPC headgroups are probably essential for driving pep46 to the membrane surface to achieve primary binding with a parallel orientation. The aggregation properties of pep46 could induce its deep insertion within the fatty acid chain region, leading to important lipid rearrangements, changes in bilayer thickness, and a decrease in the mass of the lipid bilayer due to removal of lipids. According to these results, we propose a model where pep46 adsorbs on the bilayer surface, pushes the lipid headgroups aside leading to a thinning of the membrane. pep46 could replace one layer of the lipid bilayer and could represent the first step of a membrane deformation model (Fig. 7*B*) (18).

The structure of another viral peptide with a membrane binding activity, γ peptide from flock house virus, an insect nodavirus, has been determined (21, 56–58). The amphipathic helix corresponding to the N-terminal residues (21 residues long) can disrupt membranes *in vitro* and was shown to be the host membrane-interacting region of the virus during entry (5, 57, 59). γ peptide and pep46 display similar conformations and activities.

pep46, or at least its pep22 domain, seems to behave like other surface-oriented peptides, including pro-apoptotic peptides such as Bax (60) hunter-killer peptides (61) as well the antimicrobial peptides, such as gramicidin (62), magainin (63, 64), PGLa (65), piscidin (66), and LL-37 (67). In aqueous solutions, these peptides adopt a random coil conformation and an amphipathic helical structure in both organic solvents and detergent micelles (25, 66, 68–71). NMR experiments, fluorescence quenching, and calorimetry experiments on these antimicrobial peptides at low concentration indicate that the helix is oriented parallel to the bilayer surface (64, 66, 67, 72). It has been shown by molecular dynamics simulations that a single peptide binding to the interface is not enough for pore formation (73). The amphipathic peptides bind to membranes and form pores when the required concentration is reached inducing membrane thinning, which consequently leads to pore formation (74–79). For example, melittin has been found to bind to lipid membranes in monomeric form (80), but it may self-associate at a higher concentration. Multimerization could also play a role in membrane defect formation under some conditions (81, 82). However, at higher concentrations, oriented CD spectroscopy indicated that this peptide may be oriented perpendicular to the bilayer surface (76, 83). The release of the 780 copies of pep46 present in the IBDV particle (19) within an endosome is probably sufficient to induce aggregation and pore formation.

The toroidal pore mechanism has been proposed for a series of antimicrobial peptides, *e.g.* magainin (84), melittin (85), pleurocidin (86), syringomycin (87), LL-37 (88), and cathelicidin (89), but accumulation of peptide may, as for melittin, lead to a detergent-like disintegration of the bilayer structure via a carpet mechanism (90). We can foresee that the N-terminal domain of pep46 (pep22), depending on its concentration, behaves as the antimicrobial peptides described above, with formation of toroidal pores. As already described in the case of reovirus (6), the pores are of insufficient size (around 10 nm) for the passage of a virus particle. Indeed, the pores formed by pep46 are 10 times smaller than the IBDV particle (700 Å diameter) (19). Like others, we showed for reoviruses (27) that osmotic protection of the cells depends on PEG size. PEGs large enough do not pass through the pores, retaining water on the outside and preventing cell lysis. As already discussed (27), the pore formation is a necessary step resulting in the endosome degradation by influx of water.

Our data allow us to propose a model for the entry of IBDV into cells. First, the release of pep46 from the capsid allows pep46 to interact with the endosomal membrane. The interaction of pep46 with the lipid polar heads induces a conformational change of pep46 that allows the helical structure adopted by the N-terminal amphipathic region to penetrate the lipid bilayer. The high hydrophobic domain pep46(20–32) leads to the aggregation of pep46, which subsequently induces the formation of pores in the membrane. Although the C-terminal domain was shown to modulate pep46 activity, no specific

activity has been assigned so far to this domain. The flexibility of the pep46(23–27) loop could explain the interaction of pep46 with membranes through its N terminus, and its C terminus could be responsible for the pep46 oligomerization leading to larger pores.

REFERENCES

1. Poranen, M. M., Daugelavicius, R., and Bamford, D. H. (2002) *Annu. Rev. Microbiol.* **56,** 521–538
2. Schneemann, A., Zhong, W., Gallagher, T. M., and Rueckert, R. R. (1992) *J. Virol.* **66,** 6728–6734
3. Zlotnick, A., Reddy, V. S., Dasgupta, R., Schneemann, A., Ray, W. J., Jr., Rueckert, R. R., and Johnson, J. E. (1994) *J. Biol. Chem.* **269,** 13680–13684
4. Arnold, E., Luo, M., Vriend, G., Rossmann, M. G., Palmenberg, A. C., Parks, G. D., Nicklin, M. J., and Wimmer, E. (1987) *Proc. Natl. Acad. Sci. U.S.A.* **84,** 21–25
5. Bong, D. T., Steinem, C., Janshoff, A., Johnson, J. E., and Reza Ghadiri, M. (1999) *Chem. Biol.* **6,** 473–481
6. Ivanovic, T., Agosto, M. A., Zhang, L., Chandran, K., Harrison, S. C., and Nibert, M. L. (2008) *EMBO J.* **27,** 1289–1298
7. Arias, C. F., Romero, P., Alvarez, V., and López, S. (1996) *J. Virol.* **70,** 5832–5839
8. Estes, M. K., Graham, D. Y., and Mason, B. B. (1981) *J. Virol.* **39,** 879–888
9. Greber, U. F., Webster, P., Weber, J., and Helenius, A. (1996) *EMBO J.* **15,** 1766–1777
10. Da Costa, B., Chevalier, C., Henry, C., Huet, J. C., Petit, S., Lepault, J., Boot, H., and Delmas, B. (2002) *J. Virol.* **76,** 2393–2402
11. Chandran, K., Farsetta, D. L., and Nibert, M. L. (2002) *J. Virol.* **76,** 9920–9933
12. Ruiz, M. C., Cohen, J., and Michelangeli, F. (2000) *Cell Calcium* **28,** 137–149
13. Odegard, A. L., Chandran, K., Zhang, X., Parker, J. S., Baker, T. S., and Nibert, M. L. (2004) *J. Virol.* **78,** 8732–8745
14. Nibert, M. L., Odegard, A. L., Agosto, M. A., Chandran, K., and Schiff, L. A. (2005) *J. Mol. Biol.* **345,** 461–474
15. Cohen, J. (1975) *Biochem. Biophys. Res. Commun.* **62,** 689–695
16. Spies, U., Müller, H., and Becht, H. (1987) *Virus Res.* **8,** 127–140
17. Birghan, C., Mundt, E., and Gorbalenya, A. E. (2000) *EMBO J.* **19,** 114–123
18. Galloux, M., Libersou, S., Morellet, N., Bouaziz, S., Da Costa, B., Ouldali, M., Lepault, J., and Delmas, B. (2007) *J. Biol. Chem.* **282,** 20774–20784
19. Coulibaly, F., Chevalier, C., Gutsche, I., Pous, J., Navaza, J., Bressanelli, S., Delmas, B., and Rey, F. A. (2005) *Cell* **120,** 761–772
20. Chevalier, C., Galloux, M., Pous, J., Henry, C., Denis, J., Da Costa, B., Navaza, J., Lepault, J., and Delmas, B. (2005) *J. Virol.* **79,** 12253–12263
21. Maia, L. F., Soares, M. R., Valente, A. P., Almeida, F. C., Oliveira, A. C., Gomes, A. M., Freitas, M. S., Schneemann, A., Johnson, J. E., and Silva, J. L. (2006) *J. Biol. Chem.* **281,** 29278–29286
22. Bubeck, D., Filman, D. J., Cheng, N., Steven, A. C., Hogle, J. M., and Belnap, D. M. (2005) *J. Virol.* **79,** 7745–7755
23. Wiethoff, C. M., Wodrich, H., Gerace, L., and Nemerow, G. R. (2005) *J. Virol.* **79,** 1992–2000
24. Bazzo, R., Tappin, M. J., Pastore, A., Harvey, T. S., Carver, J. A., and Campbell, I. D. (1988) *Eur. J. Biochem.* **173,** 139–146
25. Gesell, J., Zasloff, M., and Opella, S. J. (1997) *J. Biomol. NMR* **9,** 127–135
26. de Rocquigny, H., Ficheux, D., Gabus, C., Fournié-Zaluski, M. C., Darlix, J. L., and Roques, B. P. (1991) *Biochem. Biophys. Res. Commun.* **180,** 1010–1018
27. Agosto, M. A., Ivanovic, T., and Nibert, M. L. (2006) *Proc. Natl. Acad. Sci. U.S.A.* **103,** 16496–16501
28. Reid, C., and Rand, R. P. (1997) *Biophys. J.* **73,** 1692–1694
29. Freedman, J. C., and Hoffman, J. F. (1979) *J. Gen. Physiol.* **74,** 157–185
30. Griesinger, C., Otting, G., Wüthrich, K., and Ernst, R. R. (1988) *J. Am. Chem. Soc.* **110,** 7870–7872
31. Jeener, J., Meier, B. H., Bachmann, P., and Ernst, R. R. (1979) *J. Chem. Phys.* **71,** 4546–4553
32. Piotto, M., Saudek, V., and Sklenár, V. (1992) *J. Biomol. NMR* **2,** 661–665
33. Nilges, M., Clore, G. M., and Gronenborn, A. M. (1988) *FEBS Lett.* **239,** 129–136
34. Brünger, A. T., Adams, P. D., Clore, G. M., DeLano, W. L., Gros, P., Grosse-Kunstleve, R. W., Jiang, J. S., Kuszewski, J., Nilges, M., Pannu, N. S., Read, R. J., Rice, L. M., Simonson, T., and Warren, G. L. (1998) *Acta Crystallogr. D. Biol. Crystallogr.* **54,** 905–921
35. Damberg, P., Jarvet, J., and Gräslund, A. (2001) *Methods Enzymol.* **339,** 271–285
36. Beswick, V., Guerois, R., Cordier-Ochsenbein, F., Coïc, Y. M., Tam, H. D., Tostain, J., Noël, J. P., Sanson, A., and Neumann, J. M. (1999) *Eur. Biophys. J.* **28,** 48–58
37. Salamon, Z., Huang, D., Cramer, W. A., and Tollin, G. (1998) *Biophys. J.* **75,** 1874–1885
38. Mueller, P., and Rudin, D. O. (1968) *Nature* **217,** 713–719
39. Salamon, Z., and Tollin, G. (2004) *Biophys. J.* **86,** 2508–2516
40. Quijano, J. C., and Lemeshko, V. V. (2008) *Biochim. Biophys. Acta* **1778,** 2775–2780
41. Vinogradova, O., Sönnichsen, F., and Sanders, C. R., 2nd (1998) *J. Biomol. NMR* **11,** 381–386
42. Beswick, V., Roux, M., Navarre, C., Coïc, Y. M., Huynh-Dinh, T., Goffeau, A., Sanson, A., and Neumann, J. M. (1998) *Biochimie* **80,** 451–459
43. Schwarzinger, S., Kroon, G. J., Foss, T. R., Wright, P. E., and Dyson, H. J. (2000) *J. Biomol. NMR* **18,** 43–48
44. Pashkov, V. S., Maslennikov, I. V., Tchikin, L. D., Efremov, R. G., Ivanov, V. T., and Arseniev, A. S. (1999) *FEBS Lett.* **457,** 117–121
45. Orekhov, V. Y., Dubovskii, P. V., Yamada, H., Akasaka, K., and Arseniev, A. S. (2000) *J. Biomol. NMR* **17,** 257–263
46. Burkhart, B. M., Gassman, R. M., Langs, D. A., Pangborn, W. A., Duax, W. L., and Pletnev, V. (1999) *Biopolymers* **51,** 129–144
47. Brown, L. R., Bösch, C., and Wüthrich, K. (1981) *Biochim. Biophys. Acta* **642,** 296–312
48. Lohner, K., and Prenner, E. J. (1999) *Biochim. Biophys. Acta* **1462,** 141–156
49. Joanne, P., Galanth, C., Goasdoué, N., Nicolas, P., Sagan, S., Lavielle, S., Chassaing, G., El Amri, C., and Alves, I. D. (2009) *Biochim. Biophys. Acta* **1788,** 1772–1781
50. Epand, R. M. (2007) *Biophys. Chem.* **126,** 197–200
51. Lauterwein, J., Bösch, C., Brown, L. R., and Wüthrich, K. (1979) *Biochim. Biophys. Acta* **556,** 244–264
52. Park, S. H., Kim, H. E., Kim, C. M., Yun, H. J., Choi, E. C., and Lee, B. J. (2002) *Biochem. J.* **368,** 171–182
53. Chia, B. C., Carver, J. A., Mulhern, T. D., and Bowie, J. H. (2000) *Eur. J. Biochem.* **267,** 1894–1908
54. Park, C. B., Yi, K. S., Matsuzaki, K., Kim, M. S., and Kim, S. C. (2000) *Proc. Natl. Acad. Sci. U.S.A.* **97,** 8245–8250
55. Terwilliger, T. C., Weissman, L., and Eisenberg, D. (1982) *Biophys. J.* **37,** 353–361
56. Fisher, A. J., and Johnson, J. E. (1993) *Nature* **361,** 176–179
57. Banerjee, M., Khayat, R., Walukiewicz, H. E., Odegard, A. L., Schneemann, A., and Johnson, J. E. (2009) *J. Virol.* **83,** 6929–6933
58. Cheng, R. H., Reddy, V. S., Olson, N. H., Fisher, A. J., Baker, T. S., and Johnson, J. E. (1994) *Structure* **2,** 271–282
59. Bong, D. T., Janshoff, A., Steinem, C., and Ghadiri, M. R. (2000) *Biophys. J.* **78,** 839–845
60. García-Sáez, A. J., Chiantia, S., Salgado, J., and Schwille, P. (2007) *Biophys. J.* **93,** 103–112
61. Plesniak, L. A., Parducho, J. I., Ziebart, A., Geierstanger, B. H., Whiles, J. A., Melacini, G., and Jennings, P. A. (2004) *Protein Sci.* **13,** 1988–1996
62. Prenner, E. J., Lewis, R. N., Kondejewski, L. H., Hodges, R. S., and McElhaney, R. N. (1999) *Biochim. Biophys. Acta* **1417,** 211–223
63. Matsuzaki, K., Harada, M., Funakoshi, S., Fujii, N., and Miyajima, K. (1991) *Biochim. Biophys. Acta* **1063,** 162–170
64. Bechinger, B., Zasloff, M., and Opella, S. J. (1993) *Protein Sci.* **2,** 2077–2084
65. Latal, A., Degovics, G., Epand, R. F., Epand, R. M., and Lohner, K. (1997) *Eur. J. Biochem.* **248,** 938–946
66. Campagna, S., Saint, N., Molle, G., and Aumelas, A. (2007) *Biochemistry* **46,** 1771–1778
67. Henzler-Wildman, K. A., Martinez, G. V., Brown, M. F., and Ramamoorthy, A. (2004) *Biochemistry* **43,** 8459–8469

68. Porcelli, F., Verardi, R., Shi, L., Henzler-Wildman, K. A., Ramamoorthy, A., and Veglia, G. (2008) *Biochemistry* **47,** 5565–5572
69. Matsuzaki, K. (1998) *Biochim. Biophys. Acta* **1376,** 391–400
70. Biggin, P. C., and Sansom, M. S. (1999) *Biophys. Chem.* **76,** 161–183
71. Cruciani, R. A., Barker, J. L., Zasloff, M., Chen, H. C., and Colamonici, O. (1991) *Proc. Natl. Acad. Sci. U.S.A.* **88,** 3792–3796
72. Glaser, R. W., Sachse, C., Dürr, U. H., Wadhwani, P., and Ulrich, A. S. (2004) *J. Magn. Reson.* **168,** 153–163
73. Sengupta, D., Leontiadou, H., Mark, A. E., and Marrink, S. J. (2008) *Biochim. Biophys. Acta* **1778,** 1004–1014
74. Lee, M. T., Hung, W. C., Chen, F. Y., and Huang, H. W. (2008) *Proc. Natl. Acad. Sci. U.S.A.* **105,** 5087–5092
75. Huang, H. W., Chen, F. Y., and Lee, M. T. (2004) *Phys. Rev. Lett.* **92,** 198304
76. Ludtke, S. J., He, K., Heller, W. T., Harroun, T. A., Yang, L., and Huang, H. W. (1996) *Biochemistry* **35,** 13723–13728
77. Yang, L., Harroun, T. A., Weiss, T. M., Ding, L., and Huang, H. W. (2001) *Biophys. J.* **81,** 1475–1485
78. Chen, F. Y., Lee, M. T., and Huang, H. W. (2003) *Biophys. J.* **84,** 3751–3758
79. Lee, M. T., Chen, F. Y., and Huang, H. W. (2004) *Biochemistry* **43,** 3590–3599
80. Altenbach, C., and Hubbell, W. L. (1988) *Proteins* **3,** 230–242
81. Hristova, K., Dempsey, C. E., and White, S. H. (2001) *Biophys. J.* **80,** 801–811
82. Takei, J., Reményi, A., Clarke, A. R., and Dempsey, C. E. (1998) *Biochemistry* **37,** 5699–5708
83. Ludtke, S. J., He, K., Wu, Y., and Huang, H. W. (1994) *Biochim. Biophys. Acta* **1190,** 181–184
84. Matsuzaki, K., Sugishita, K., Ishibe, N., Ueha, M., Nakata, S., Miyajima, K., and Epand, R. M. (1998) *Biochemistry* **37,** 11856–11863
85. Matsuzaki, K., Yoneyama, S., and Miyajima, K. (1997) *Biophys. J.* **73,** 831–838
86. Saint, N., Cadiou, H., Bessin, Y., and Molle, G. (2002) *Biochim. Biophys. Acta* **1564,** 359–364
87. Malev, V. V., Schagina, L. V., Gurnev, P. A., Takemoto, J. Y., Nestorovich, E. M., and Bezrukov, S. M. (2002) *Biophys J* **82,** 1985–1994
88. Henzler Wildman, K. A., Lee, D. K., and Ramamoorthy, A. (2003) *Biochemistry* **42,** 6545–6558
89. Basañez, G., Shinnar, A. E., and Zimmerberg, J. (2002) *FEBS Lett.* **532,** 115–120
90. Naito, A., Nagao, T., Norisada, K., Mizuno, T., Tuzi, S., and Saitô, H. (2000) *Biophys. J.* **78,** 2405–2417

NMR Structure of a Viral Peptide Inserted in Artificial Membranes: A VIEW ON THE EARLY STEPS OF THE BIRNAVIRUS ENTRY PROCESS

Marie Galloux, Sonia Libersou, Isabel D. Alves, Rodrigue Marquant, Gilmar F. Salgado, Human Rezaei, Jean Lepault, Bernard Delmas, Serge Bouaziz and Nelly Morellet

J. Biol. Chem. 2010, 285:19409-19421.
doi: 10.1074/jbc.M109.076083 originally published online April 9, 2010
